SOME DESIGN FEATURES OF SOLID PROPELLANT ROCKET MOTORS FOR SHOULDER-LAUNCHED WEAPON SYSTEMS

Berko ZECEVIC, Jasmin TERZIC, Mario BASKARAD, Alan CATOVIC, Sabina SERDAREVIC-KADIC, Zijo PEKIC,
University of Sarajevo, Mechanical Engineering Faculty, Defense Technologies Department
Vilsonovo setaliste 9 71000 Sarajevo,, Bosnia and Herzegovina

Abstract. Solid propellant rocket motors for Shoulder Launched Infantry Weapon Systems (SLWS) are characterized with very short burning time, high-pressure combustion and wide spectrum of design solutions for rocket motor structure. Interior ballistic behaviour of such rocket motors depends on many factors as design structure, propellant grain shape, propellant grain joint to the rocket motor case, type and location of the igniter, spinning mode and nozzle design. Erosive burning also plays important role due to high combustion gases mass flow rate. Numerical simulation of the igniter combustion gases flow through the hollow of the propellant grain tubes with gas temperature distribution was carried out in this paper. Results confirmed an assumptions that igniter interior gases flow affected pressure rise duration. A mathematical model approach for prediction of curve p=f(t) which was included a model of the corrected propellant grain burning surface for two types of short-time rocket motors has been presented. A good agreement with measured curves was achieved.
Keywords: short-action solid rocket motor, burning rate, ignition time, derivative *dp/dt*, regression model.

1. INTRODUCTION

An intensive development of shoulder-launched weapon systems (unguided and guided) with munitions propelled by solid propellant rocket motors has been carrying out recently. These projectiles have range of several hundred meters up to approximately 800 meters. Current shoulder fired missiles and rockets are designed primarily to defeat tanks and armored vehicles, but inadequate when fired against brick walls or fortified concrete targets.

The shoulder-fired man-portable anti-tank missile systems use usually gas generators in order to launch a rocket from launch tube or booster rocket motors that are separated after launching. Some of them have a booster rocket motor which is integrated into the missile structure. Typical representatives of shoulder-fired man-portable anti-tank missile systems are The M47 DRAGON, ERYX, The FGM-148 Javelin, Spike-SR etc.

At unguided SLWS, solid propellant grain must be burnt while a projectile is still inside the launch because of operator's safety requirements. Typical representatives of shoulder launched infantry rocket weapons are Apilas, The Shoulder-launched

Multipurpose Assault Weapon (SMAW), Light Anti-Armor Weapon or M72 LAW or 64 mm M80 Zolja or RPG-18, Light Anti-Armor Weapon LAW 80, B-300, RPG-22, RPG-26, Shipon, 90 mm M79 OSA etc.

A common feature of both SLWS is rocket motor with extremely short burning time, measured in milliseconds.

Acceleration during the launch phase makes another distinction between SLWS; guided anti-tank missiles have low acceleration when launched, and unguided infantry projectiles have acceleration of 3000-8000 g. These distinctions affect design of entire rocket motor, especially nozzle.

Design of solid propellant rocket motors for SLWS munitions is considerable more complex compared to most of rocket motors for some other purposes. Specific requirements for such rocket motors are as following:

- Short burning time;
- Launch rocket motor must not be active at the launch tube muzzle;
- High pressure inside the rocket motor chamber;
- Environmental conditions when used from -40°C up to +60°C;
- Low temperature sensitivity of the solid propellant;
- Reliable ignition;
- Short ignition time;
- Short ignition rise time;
- High safety requirements, because SLWS is fired from operator's shoulder.

Figure 1. A Soldier fires a AT-4 Weapon at a target [1]

Rocket motors for SLWS missiles have small dimensions and weight when compared to a total weight and mechanical envelope of the missile. An envelope of the rocket motor is not dominant at missile design structure.

At SLWS rocket munitions, nozzle is dominant within the envelope of the rocket motor. The following figures show characteristic mechanical envelopes of short-time combustion rocket motors, B-300 or SMAW, APILAS and ACL APX-80.

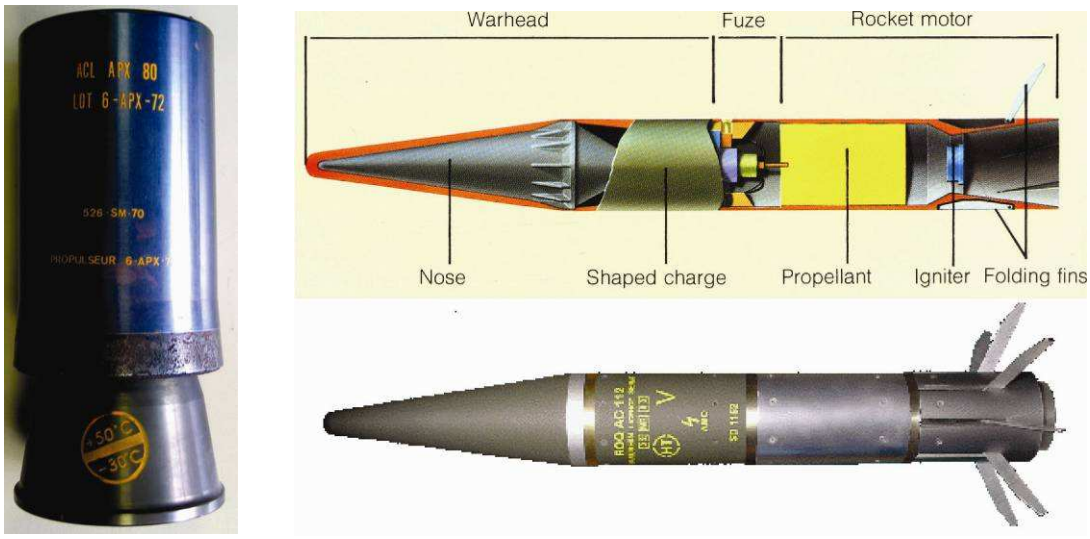

Figure 2. Rocket motor ACL APX-80 (left) and rocket motor APILAS [2] (right)

Figure 3. Rocket motor B-300 [3] (left), rocket 66 mm M72 LAW [17] (right)

It can be seen that the nozzle throat diameter is quite big, nozzle expansion ratio is low and rocket motor occupies significant part within a mechanical envelope of the entire rocket projectile. Nozzle design indicates that combustion products mass flow through the nozzle is extremely high. Such flow conditions induce erosive burning of the propellant grain particularly in the start-up phase.

High exhaust mass flow generates overpressure blast behind the launcher (Figure1.) which is specific problem when SLWS fired from closed area. This is main deficiency of most current weapons because they cannot be fired from enclosures, such as rooms or bunkers, rendering the user vulnerable to enemy fire. This problem is also important for design of short burning time rocket motors applied in SLWS.

This brief overview has described most significant influences, resulted from intended use of SLWS, on design of rocket motors.

2. PUBLISHED DATA OF SOME SHORT-ACTION SOLID PROPELLANT ROCKET MOTORS

Available published papers describing a specific methodology for designing short time rocket motors are quite rare. Mechanical Engineering Faculty, University of Sarajevo - Defense Technology Department has carried out a comparative analysis of four short burning time rocket motors in order to explore some specific design features

of rocket motors for SLWS, which would make distinction between them and general design features of tactical solid propellant rocket motors .

Two rocket motors from SLWS DRAGON (gas generator, Figure 5. and correction impulse rocket motors, Figure 4.), rocket motor 68 mm “Zolja” (similar to M72 LAW or RPG-18) and rocket motor 90 mm “OSA” were analysed in this paper.

The DRAGON is SLWS which consists of the launcher, tracker and the medium-range, wire-guided antitank missile [4]. Gas generator mounted inside the rear part of the launch tube serves as a High-Low pressure propulsion system.

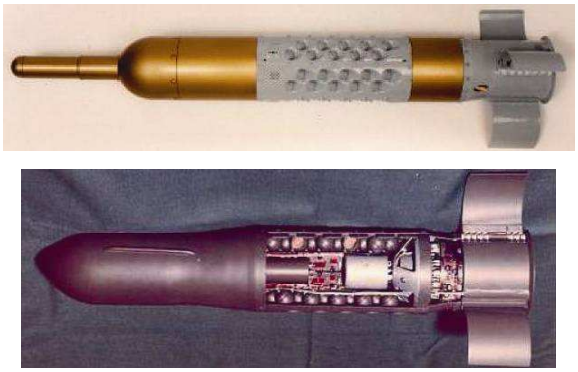

Figure 4. Impulse control rocket motors of DRAGON missile [18]

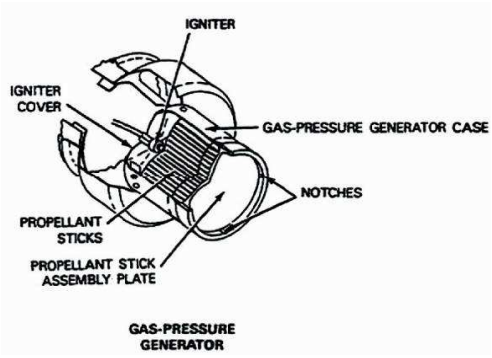

Figure 5. Gas generator of DRAGON missile[4]

]High pressure of 17-24 MPa develops inside gas generator structure, while low pressure of 1,7- 2,1 MPa is inside the launch tube. Gas generator enables launching DRAGON missile from the launch tube.

Control is performed by means of plurality of small correction impulse rocket motors mounted around cylindrical body of the missile.

Gas generator propellant grain made of M36 double base propellant is in the form of 190 tubular sticks, which are bonded to an aluminium propellant holder. The M-36 propellant have high burning rate, mesa burning characteristics over operating pressure range, low π_K, high specific impulse, it is smokeless and easily producible.

From firing test curves $p=f(t)$ for DRAGON’s gas generator conditioned at temperatures of 233 K, 294 K and 336 K (Figure 6. and 7.) following characteristics are distinct:

- Ignition delay time is quite long when compared with total action time;
- Pressure rise at start-up phase is high (*dp/dt* achieves 70 MPa/ms at temperature of 336 K, and 13 MPa/ms at temperature of 233 K).
- Ignition rise time is short (mean ignition rise time 4,398 ms for 233 K).

- Mean combustion time (action time) is between 25,43 ms (for 336 K) to 31,311 ms (for 233 K).
- Tail-off phase is significantly longer then start-up phase.

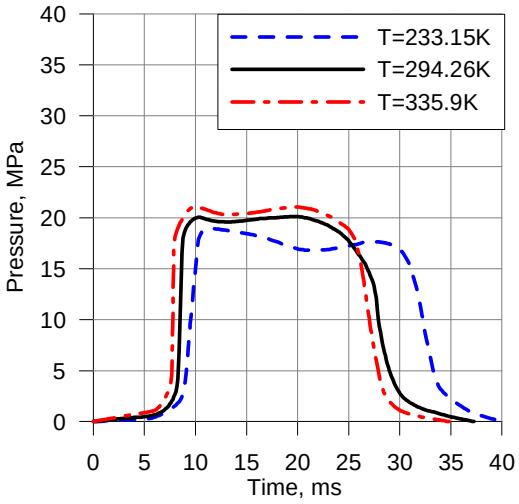

Figure 6. DRAGON gas generator pressure vs. time [4]

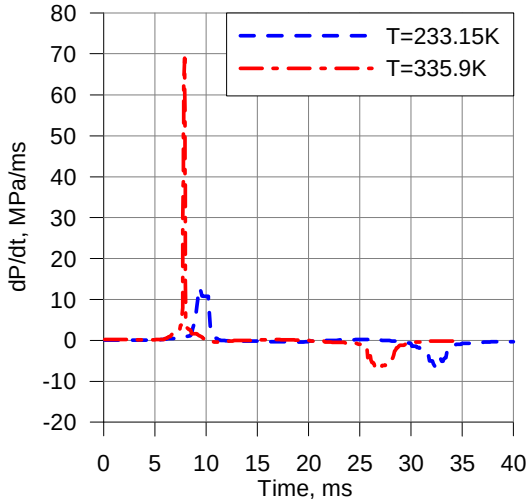

Figure 7. DRAGON gas generator dp/dt vs. time

In order to estimate specific points from pressure vs. time curve *p=f(t)*, which is used to determine ignition delay, ignition rise time, combustion time (action time) and tail-off time a digital processing of *p=f(t)* curves has been applied at Defense Technology Department. Curves *p=f(t)* were transformed into *dp/dt=f(t)*, from which all characteristic points are easier to be noted. Derived curves *dp/dt* vs. time clearly indicate characteristic phases of the rocket motor action and influence of conditioned temperatures on combustion chamber pressure variation particularly during transient start-up and tail-off phases.

Impulse rocket motors of the DRAGON missile use the same solid propellant M36 (as in the gas generator) which is formed into strips and then is rolled into scrolls. Analysing published firing test curves *p=f(t)* for conditioned temperatures 233 K, 294 K and 336 K (Figure 8.) by means of derivative *dp/dt=f(t)* (Figure 9.), following characteristics can be noticed:

- Transient processes are short when compared with total action time of the rocket motor (f. e. mean ignition delay time is 1,88 ms for 233 K);
- Pressure rise at start-up phase is also high (*dp/dt* achieves 65 MPa/ms at temperature of 336 K, and 17 MPa/ms at temperature of 233 K);

- Ignition rise time for all temperatures is extremely short (mean ignition rise time is 0,69 ms at 233 K);
- Mean combustion time (action time) is 24,16 ms (for 233 K) to 18,60 ms (at 336 K);
- Peak pressure of 36,21 MPa, occurred at the end of burning at temperature of 336 K, was most likely caused by cracking of the solid propellant grain, because there were no same occurrence at another two conditioned temperatures;
- Although the propellant type is the same as in the gas generator with similar webs (1,04 mm vs. 1,17 mm), a higher sensitivity to temperature was noticed when compared with gas generator pressure-time behaviour. It means that solid propellant grain shape, rocket motor design structure and burning conditions affect burning process.
- Derived curves *dp/dt* vs. time also indicate characteristic phases of the rocket motor action and considerable influence of conditioned temperatures on combustion chamber pressure variation particularly during transient start-up and tail-off phases.

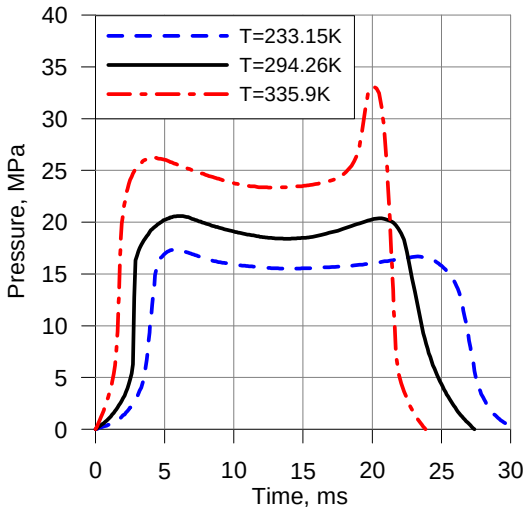

Figure 8. DRAGON impulse control rocket motor pressure vs. time [4]

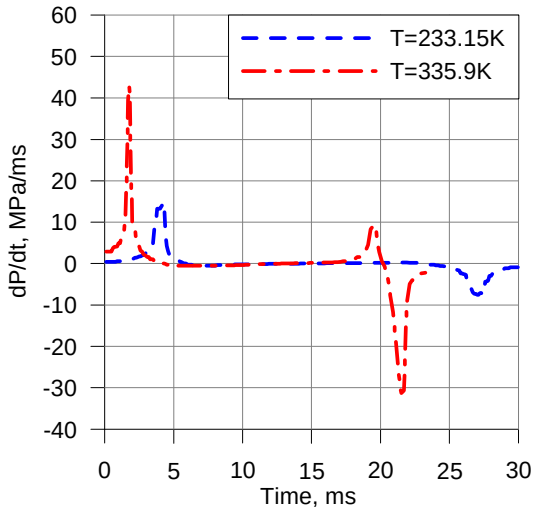

Figure 9. DRAGON impulse control rocket motor dp/dt vs. time

Ignition delay (time when 10% of initial peak pressure is achieved) is determined by burst diaphragm design features. Greater thickness of the burst diaphragm can cause combustion oscillations, unforeseen peak pressure and even solid propellant grain to be cracked. Thinner burst diaphragm could affect harder ignition particularly at lower temperatures as 233 K, so this problem should be taken into consideration when a new rocket motor is designed.

Since more detailed design data about above described rocket motors were not

available for further analysis, our efforts were focused on SLWS rocket motors with known design features. These are two SLWS rocket motors using double base propellants with almost the same propellant composition but with different propellant grains.

Rocket motor of the rocket 64 mm HEAT M80 (Figure 10.) contains solid propellant grain made of double base propellant NGR-124, which is in the form of multiple-tube grain with 37 tubular sticks bonded to an aluminium propellant holder.

Figure 10. Rocket motor 64 mm M80 (above [19]) and its multiple tube grain (down)

By analysing firing test curves *p=f(t)* for conditioned temperatures 243 K, 294 K and 323 K using derivative *dp/dt=f(t)*, following characteristics can be noticed (Figure 11.):

- A strong temperature sensitivity of the propellant to temperature is obvious - action time of the rocket motor is about 10 ms at conditioned temperature of 243K and about 5 ms at 323K;
- Ignition rise time is quite long and it is almost as web burning time;
- Start-up pressure rise is quite unusual at temperature of 233 K;
- During ignition phase, maximum value of *dp/dt* at temperature of 323K is 38 MPa/ms, while it is only 5 MPa/ms at 223 K;
- Pressure rise at start-up phase is pretty modest at 233 K, which means that ignition process was not optimal for design structure of the rocket motor (burst diaphragm adhesive joint affects ignition process at various temperatures, which is outstanding at low temperatures);
- Tail-off time is less then start-up ignition rise time, which is unusual for rocket motors.

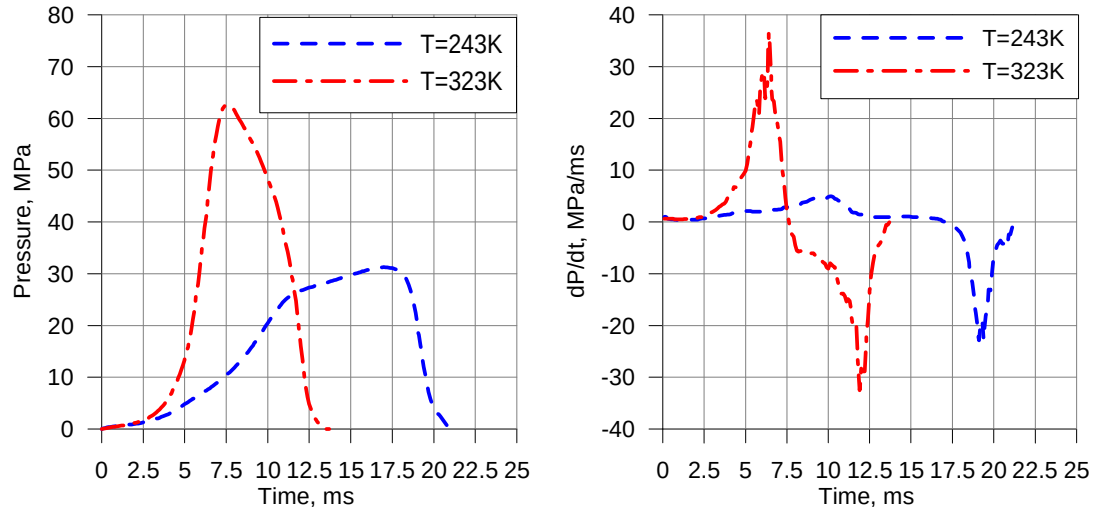

Figure 11. Pressure vs. time curve and dp/dt vs. time for rocket motor of 64 mm HEAT M80

Burning process is affected by grain geometry and propellant type, rocket motor chamber design, ignition case, mass and type of ignition charge etc.

Rocket motor of the rocket 90 mm HEAT M79 (Figure 12.) contains solid propellant grain made of double base propellant NGR-114, which is in the form of multiple-tube grain with 121 tubular sticks bonded to an aluminium propellant holder.

Figure 12. Rocket motor 90 mm M79 (left) and its propellant grain, hollow cylindrical type (right)

By analysing firing test curves p=f(t) for conditioned temperatures 243 K, 294 K and 323 K using derivative dp/dt=f(t) (Figure 13.), following characteristics of this rocket motor can be noticed:

- High temperature sensitivity reflecting through the rocket motor action time (about 13 ms at 243 K and about 7 ms at temperature of 313 K);
- Ignition rise time is quite long when compared with total burning time, particularly at temperature of 313 K;
- Maximum value of *dp/dt* at temperature of 313 K at start-up phase is 33 MPa/ms, while it is 19 MPa/ms at 243 K;

- Tail-off phase time is unusually long at temperature 243 K, indicating that rocket motor design was not optimised;
- Pressure rise at start-up phase is quite slow at 243 K, which also means that ignition process was not optimal for design structure of the rocket motor;
- Tail-off phase time at temperature of 243 K is distinctly long and variation of derivative *dp/dt* behaves unexpectedly.

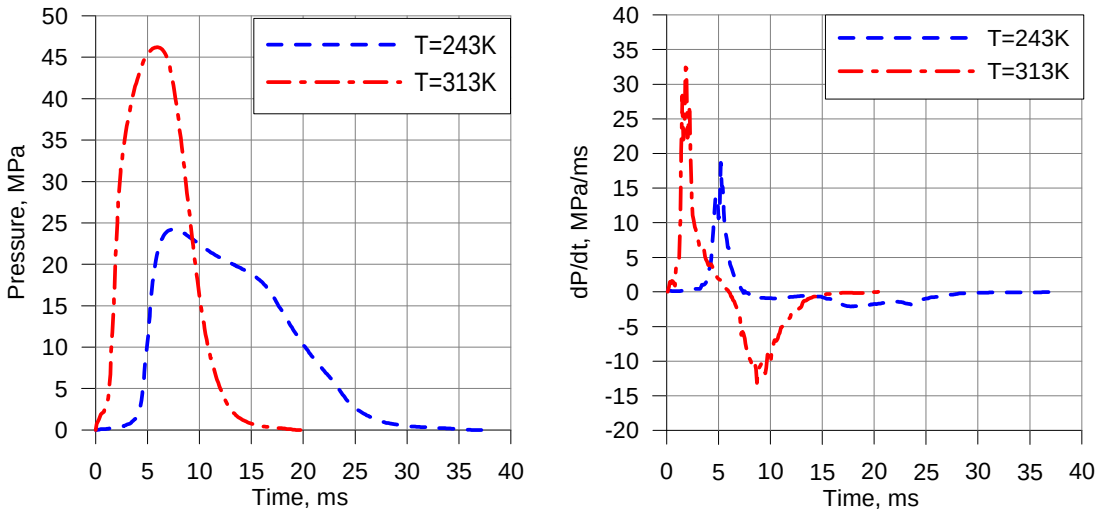

Figure 13. Pressure vs. time and dp/dt vs. time for the rocket motor of 90 mm HEAT M79

Solid propellant composition, shape and dimensions of the propellant grain for both rocket motors are very similar, but considerable variations in the interior ballistic processes were noticed. As already mentioned, the long start-up phase at rocket motor 64 mm „Zolja“ (at temperature of 243 K) indicates a considerable influence of the igniter as well as entire rocket motor design on interior ballistic of short-action rocket motors. Therefore, it is important to explore an influence of erosive burning (during the start-up phase), temperature sensitivity of the propellant, ignition process and design of interior rocket motor structure on interior ballistics of these rocket motors.

3. ANALYSIS OF ROCKET MOTORS 64 MM M80 AND 90 MM M79

Short-Action solid propellant rocket motors are characterized by short burning time, high propellant loading density and significant influence of erosive burning at start-up phase.

In order to explore an influence of some parameters on interior ballistics of short-time rocket motors it is necessary to determine the burning rate law using ballistic evaluation motors, as well as using actual rocket motors (where erosive burning is

included), including ratios $K=A_b/A_{th}$ (where A_b = burning propellant surface, A_{th} = nozzle throat area), $K_i=A_b/A_p(x)$ ($A_p(x)$=Cross-sectional area or port area available for the downstream gas flow) and $J= A_{th}/A_p(x)$.

For rocket motors with high loading density the total port area in the grain available for the downstream gas flow usually becomes very small, however, there is a certain limit that must be taken into account to avoid burning instabilities. This geometrical condition is most important at the beginning of the combustion process because the total port area of the grain is minimal and can be characterized by the value of $K_i =A_b/A_p(x)$. After ignition, an initial value for K_i should be limited to $J_i=K_i/K < 0,6$ in order to avoid burning instabilities.

For a multiple-tube grain the definition of the different values for K_i can be helpful to characterize the axial flow in the combustion chamber, the first of which is formulated with the total cross-section port area, the second with all wedge shaped cross-sections between the tubes and the third, generally the most critical one, with the port area of a single tube and the appropriate burning surfaces which generate the local downstream gas flow [5].

The basic multiple-tube grain configuration can be found and optimised by using a special Dynamit Nobel computer code which includes the grain geometry related aspects of internal ballistics and offers the user a choice of geometrical tube arrangements. Multiple-tube arrangement in combustion chambers with ring-shaped cross-section can also be handled with this code.

Tabele 1. Multiple-Tube Grain Design Parameter.

No. tubes	x	Lading factor
3	2,155	0,6462
4	2,414	0,6864
5	2,701	0,6852
(6	3,000	0,6667)
7	3,000	0,7778
8	3,306	0,7320
9	3,613	0,6895
10	3,924	0,6494
(11	4,236	0,6130)
12	4,232	0,6700
13	4,236	0,7244
15	4,552	0,7238
19	4,864	0,8031
28	6,127	0,7459

For tubes arranged on concentric circles the inner diameter R of a rocket motor case can be easily expressed as a function of the grain tube diameter *r*. Table 1 contains this relationship ($R = r \cdot x$) together with the loading factor [5].

3.1 Solid propellant burning rate at actual rocket motors

Propellant burning rate is mostly influenced by the combustion chamber pressure and is expressed by Saint Robert's (or Vielle's) law within a limited pressure range:

$$r = a \cdot p^n \tag{1}$$

The pressure exponent n and the burn rate coefficient a are dependent on chemical composition of a solid propellant and initial temperature of the propellant grain. These coefficients are usually determined by means of firing test of ballistic evaluation motors [6,7,8,9,10].

Applied shapes of solid propellant grains for standard ballistic evaluation motors should ensure a low flow velocity over the burning surface, or mass flux of combustion products through the internal flow channel. The pressure exponent n should be independent on the combustion chamber pressure at a defined pressure range, and should be valid for a defined initial grain temperature.

Burning rate measured by ballistic evaluation motors must be corrected for actual rocket motors, which depends on rocket motor size and conditions of its application. In order to obtain actual values of burning rates within a rocket motor, previous measured values should be fitted for an actual rocket motor. Typical fitting coefficient of burning rates, which is applicable to actual rocket motors, lies between values of 1,01 to 1,05 [7].

Burning rate laws of double base propellant NGR 114 (Figure 14.) measured in the standardized ballistic evaluation motor 32/16 at different temperatures are very close to burning rate laws of double base propellant NGR 124.

Actual burning rate within real rocket motors is under other influences and because of that the burning rate is one of ballistic properties, which is determined with difficulty.

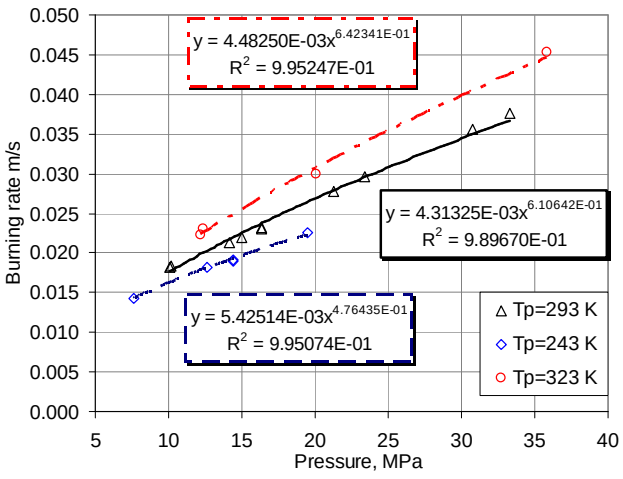

Figure 14. Burning rate laws of the propellant NGR-114 measured in the standardized ballistic evaluation motor type 32/16

An actual burning rate in a rocket motor, except the basic value measured in standard ballistic evaluation motors, consists of several components.

Determination of these components is a very complex task because many assumptions must be included to estimate their influence on the total actual burning rate.

Estimation of variation of the basic burning rate due to influence of several factors can be made by appropriate separation each of influence components. Researches of the influence of gaseous mass flux on the basic burning rate, which was performed by many authors [11,7], show that combustion products flow over the burning surface causes erosive burning [12,13].

Influence of mass flux or erosive burning on burning rate in rocket motor chamber is considered using modified formula of Lenoir and Robillard (LR). In this model total burning rate contains component of burning rate in normal burning (no erosive burning) r_0 and component which is result of erosive burning r_e [14,20]:

$$r_i = r_0 + r_e \tag{2}$$

The LR model defines the erosive burning contribution as:

$$r_e = \alpha \cdot G^{0,8} \cdot \exp\left(-\beta \cdot r_b \cdot \rho_s / G\right) / L^{0,2} \tag{3}$$

$$\alpha = \frac{0.0288 \cdot c_{p_g} \cdot \mu_g^{\,0,2} \cdot \mathrm{Pr}_g^{-2/3}}{\rho_s \cdot c_s} \cdot \left(\frac{T_c - T_s}{T_s - T_0}\right) \tag{4}$$

where G – the mass flux of the combustion gasses, ρ_s – density of propellant [kg/m^3], L – characteristic length [m], c_{pg} – constant pressure specific heat of gasses [J/kgK], Pr – Prandtl number, T_c , T_s ,T_0 - temperature of combustion products, burning surface and initial condition of propellant [K], c_s – constant pressure specific heat of propellant [J/kgK]. Using equations 3 and 4, the erosive burning contribution can be calculated using only one empirical value (β), which is essentially independent of propellant composition and approximately 53 [14,20]. The value of in equation 4 can also be assigned from empirical data rather than calculated with transport properties.

Pressure-time predictions for rocket motors 90 mm M79 and 64 mm M80 were performed using software SPPMEF. Basic burning rate laws of double base propellants NGR 114 and NGR 124 measured in standardized ballistic evaluation motors type 32/16 (the same burning law for both propellants) were used as an input.

Influence of erosive burning was not included in first prediction. Considerable deviations of the pressure and burning time were obtained at 243 K (curves *p=f(t)* with interrupted line) relative to measured values (curves *p=f(t)* with full line).

When the influence of erosive burning is taken into account (coefficient $J=A_{th}/A_p \approx 0.51$) for both rocket motors, following coefficients values were used $\beta=65$ (for rocket motor 64 mm HEAT M80) and $\beta=80$ (for rocket motor 90 mm HEAT M79), significant curve changes *p=f(t)* were obtained, comparing to first predictions (Figures 15. and 16.). For rocket motor 64 mm HEAT M80 there are certain differences in the character of prediction and experimental curve *p=f(t)*, and this difference is a result of ignition process under low temperatures, while for rocket motor 90 mm HEAT M79 curves *p=f(t)* are very similar.

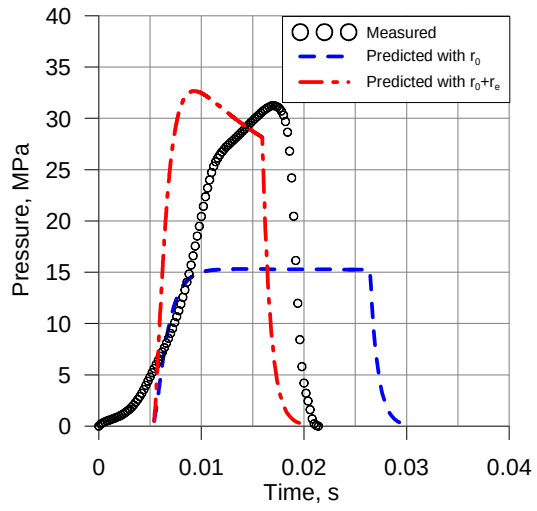

Figure 15. Pressure vs. time prediction compared with measured curve for 64 mm HEAT M80 at temperature 243 K

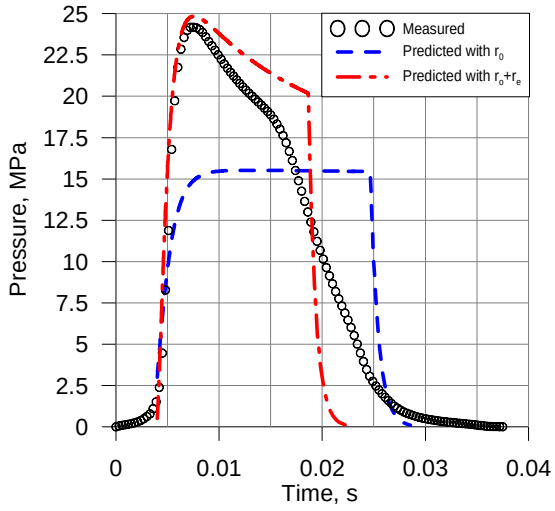

Figure 16. Pressure vs. time prediction compared with measured curve for 90 mm HEAT M79 at temperature 243 K

Characteristic difference between predicted and measured curves was also confirmed by pressure vs. time prediction at temperature of 323 K.

Computer code SPPMEF, which was used for these simulations, represents a reliable tool for solid propellant rocket motor performances prediction [15].

Pressure variation in the rocket motor chamber as a function of time is predicted using following equation:

$$\frac{dp_c}{dt} = \frac{1}{V_{c_i}} \cdot \left[R_g \cdot T_c \cdot \left(\sum_{i=1} \rho_p \cdot A_{b_i} \cdot r_i - \frac{p_{c_i} \cdot A_{th_i}}{C^*} \right) - p_{c_i} \cdot \frac{dV_{c_i}}{dt} \right] \tag{5}$$

Analysis of equation (4) and curves $p=f(t)$ for rocket motors 64 mm M80 and 90 mm M79 at extreme temperatures shows:

- A crucial influence on pressure variation have the grain burning surface A_{bi} and actual propellant burning rate r_i , while free volume V_{ci} considerable less affects interior ballistic process of the rocket motors.
- Short-action rocket motor structure and solid propellant grain design play important roles during interior ballistic cycle of the rocket motor.
- Deviation of measured curves $p=f(t)$ from predicted curves obtained when the computer code SPPMEF was used, is result of grain burning surface A_{bi}, and actual propellant burning rate r_i variations (which reflects through erosive burning at some particular zones inside the chamber). This occurs at both rocket motors and during entire burning process.

Therefore a detailed analysis of all action phases, from start-up until tail-off phase was analysed. These deviations can be explained with significant variations of actual solid propellant grain surface A_{bi} when compared with the usual geometric propellant grain burning surface regression model.

A hypothesis that explains mentioned deviations is based on following assumptions:

- During the start-up phase, combustion gases generated by the igniters do not ignite entire grain surface simultaneously because gaseous flow cannot reach farther zones of inner and outer surfaces of the propellant grain tubes;
- Due to influence of erosive burning, propellant grain burning surface regression model must be changed to include such phenomenon;
- Tail-off phase curve deviation occurs because thin partially burned grain tubes are cracked.

In order to confirm this hypothesis a numerical simulation of gaseous flow through the hollow of the propellant grain tubes with gas temperature distribution was carried out. Two cases were considered, one with open tube ends and another with one plugged end. Computer code COMET [16] was applied for these simulations.

Results of such simulations (Figure 17.) show that a hot gaseous flow reached opposite end of the propellant tube in approximately 9 ms at combustion chamber pressure of 9 MPa. Since the total burning time for analysed rocket motor is about 15 ms, it is obvious that igniters gaseous flow duration in the combustion chamber

considerable affect interior ballistic process in the short-action rocket motors. Hot gaseous flow at open propellant grain tube reached opposite end in about 6 ms.

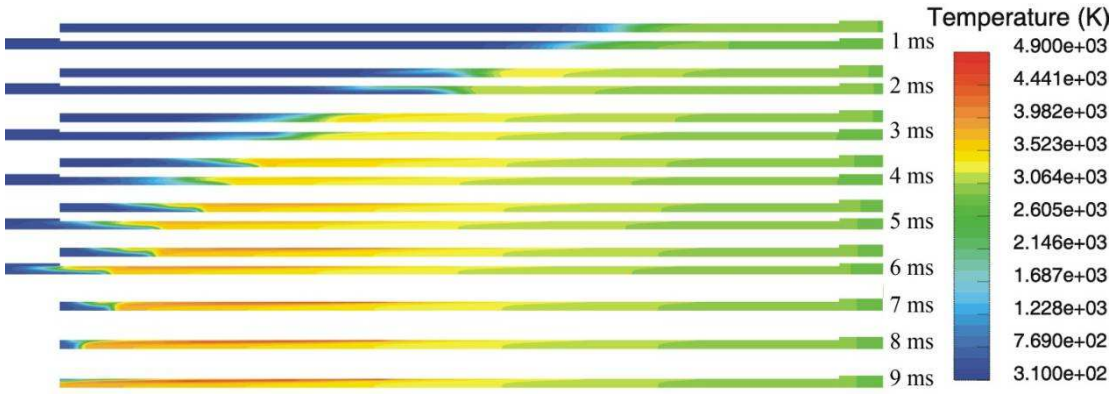

Figure 17. Hot gaseous flow reach and temperature distribution inside a hollow of tubular propellant grains (for one-end plugged and open propellant tube)

These simulations clearly indicated that certain delay of ignition at some farther zones of the propellant grain surfaces significantly affects start-up pressure vs. time curve.

3.2 A model of the corrected propellant grain burning surface

Rocket motors with high propellant loading factor have also “smothered” burning at outer propellant grain burning surfaces. Presented model of the corrected grain burning surface was based on following assumptions:

- Start-up phase of short-action rocket motors is time-consuming process that needs more time for entire propellant grain surface to be spread with igniter combustion gases. During this transient process only a certain part of the propellant grain surface is burned and other part of the grain is not yet included into burning process. It was assumed therefore that total propellant grain surface was ignited when the flame front passed a web burned distance w_i. Length correction of the hollow cylindrical propellant grain (L_0) for inner (L_i^i) and outer (L_i^0) surface was done by means of coefficients k_1 and k_2.
- Total propellant grain surface was spread by the flame when web burned distance was achieved a value of $w_i \geq k_3 \cdot w_0$. This moment was defined by the coefficient k_3.
- Period defined with coefficient k_4=1, when instantaneous length of the inner and outer burning surfaces of a hollow cylindrical grain became equal.

- A considerable change of burning surface length occurred at certain moment ($k_4(w_i)<1$), as shown in Figure 18, because of erosive burning at start-up phase and non-uniform flame spread along the propellant grain.
- Deviation of the tail-off phase was caused by increased burning surface occurred due to cracks of thin propellant grain remains. Eccentricity of propellant tubes and small web also created conditions for cracks to be occurred. This also affected the total impulse of the rocket motors.

Burning surface varies in accordance with following regression model:

$$A_{b_i} = A^o_{b_i} + A^i_{b_i} \tag{5}$$

$$A^o_{b_i} = d_{o_i} \cdot \pi \cdot n \cdot L^o_i \quad and \quad A^i_{b_i} = d_{i_i} \cdot \pi \cdot n \cdot L^i_i \tag{6}$$

$$d_{o_i} = (d_o - 2 \cdot w_i) \quad and \quad d_{i_i} = (d_i + 2 \cdot w_i) \tag{7}$$

$$w_i = \sum r_i \cdot \Delta t_i \tag{8}$$

$$L^o_i = L^o_0 \cdot k_1 - w_i \quad and \quad L^i_i = L^i_0 \cdot k_2 - w_i \tag{9}$$

Where is $k_1(w_i) \le 1$ *and* $0 < k_2(w_i) \le 1$ *for* $w_i \le k_3 \cdot w_0, \quad k_3(w_i) \ge 0$

For $w_i \ge k_3 \cdot w_0 \quad and \quad k_4 = 1$

$$L^o_i = L^i_i = (L_0 - w_i) \tag{10}$$

For $k_3 \cdot w_0 < w_i \le w_0 \quad and \quad k_4(w_i) < 1$

$$L^o_i = L^i_i = \frac{w_0 \cdot (1 - k_3 \cdot k_4) - w_i \cdot (1 - k_4)}{(1 - k_4) \cdot w_0} \cdot (L_0 - w_i) \tag{11}$$

Figure 18. shows form of the propellant grain burning surface vs. web burned distance according to presented model.

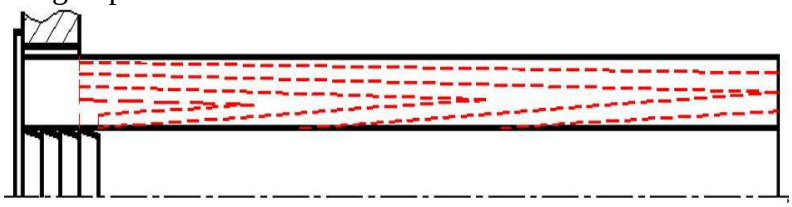

Figure 18. Propellant grain burning surface regression model

Using above described model of propellant grain burning surface change for short-action rocket motors, numerical simulation of curve *p=f(t)* for rocket motors 64 mm M80 „Zolja“ and 90 mm M79 „Osa“ has been performed.

For simulation of the rocket motor 64 mm M80 „Zolja“, coefficients $k_1(w_i)$=0,3-1,0, $k_2(w_i)$= 0,3-1,0 (outer propellant grain burning surface was corrected), k_3=0,15 and k_4=1,0. Within web range of $k_3 \cdot w_0 < w_i \le 0.5 \cdot w_0$ (for temperature 243 K ≤ w_0) coefficient k_4=1, and later coefficient $k_4(w_i)$ linearly decreased to the value of k_4=0,8. For

temperature 243 K coefficient $\beta=65$, and for temperature 323 K coefficient $\beta=58$. Obtained functions $p=f(t)$ were very similar to actually measured curves at temperatures of 243 K and 323 K. These agreements are shown in Figure 19 and Figure 20.

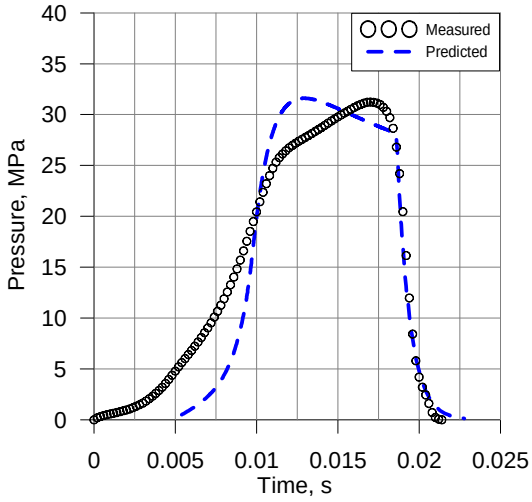

Figure 19. Comparison of predicted and measured curves at 243 K - 64 mm M80 „Zolja“

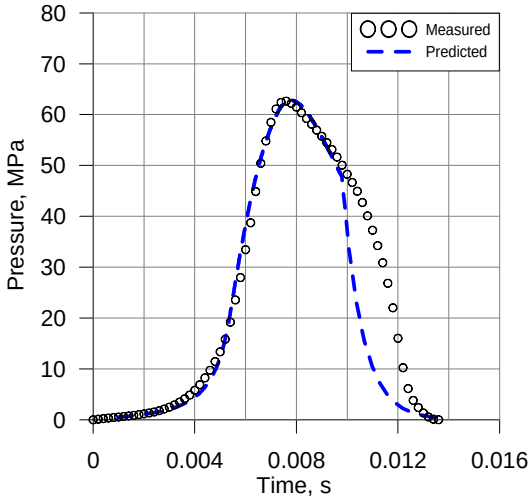

Figure 20. Comparison of predicted and measured curves at 323 K - 64 mm M80 „Zolja“

There were certain disagreements at tail-off phase, although further improvement of the corrected propellant grain burning surface model offers an opportunity to achieve better agreements even in this phase.

For simulation of the rocket motor 90 mm M79 „Osa“, coefficients $k_1(w_i)$=0,3-1,0, k_2=1, k_3=0,15 and k_4=1,0 (outer propellant grain burning surface was not corrected). Within web range of $k_3 \cdot w_0 < w_i \leq 0.7 \cdot w_0$ coefficient k_4=1, and later coefficient $k_4(w_i)$ linearly decreased to the value of k_4=0,75. For temperature 243 K coefficient $\beta=80$ and for temperature 313 K coefficient $\beta=94$.

Figures 21 and 22 show good agreements of predicted curves with measured at 243 K and 313 K. As already mentioned, although there were similar disagreements at tail-off phase, it is possible to achieve better results with further improvement of the corrected propellant grain burning surface model.

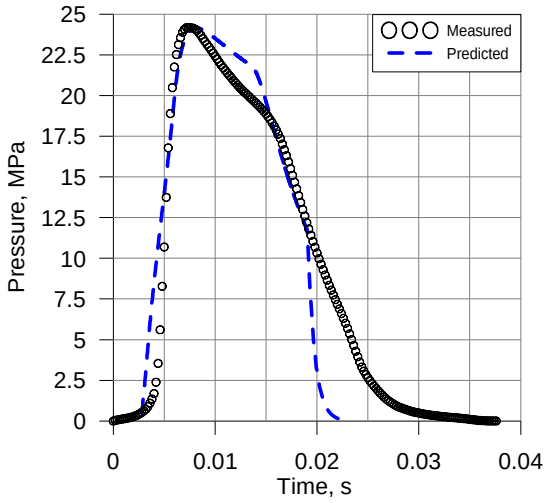

Figure 21. Comparison of predicted and measured curves at 243 K - 90 mm M79 „Osa“.

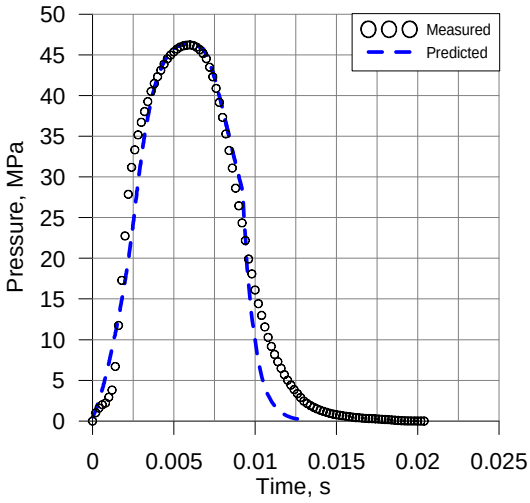

Figure 22. Comparison of predicted and measured curves at 313 K - 90 mm M79 „Osa“.

As illustrated, predictions for a case when length of the outer propellant grain burning surface was not changed were carried out (interrupted line). A considerable deviation of $p=f(t)$ from measured curve can be noticed (Figure 21.).

In this analysis, total burning surface and cross-sectional throat area ratio represented by K has value of $K = 350$ for rocket motor 64 mm M80 „Zolja“, and K=326 for rocket motor 90 mm M79 „Osa“.

The other design ratio J ($J \approx 0{,}52$) for both rocket motors is quite high indicting occurrence of intensive erosive burning.

Gaseous flow velocities at the port zone in the beginning of propellant grain burning were calculated and their values were about 540 m/s for rocket motor 90 mm M79 „Osa“ and about 440 m/s for rocket motor 64 mm M80 „Zolja“. These values indicate how important role plays mass flow rate for interior ballistic process of both rocket motors.

For prediction of curve $p=f(t)$ for both impulse rocket motors it is not possible to use burning rate determined in standardized ballistic evaluation motors 32/16. It is necessary to take into consideration component of erosive burning rate (equations 2, 3, 4) and take into account gas-dynamic effects for specific configuration of propellant charge (non-uniform burning in space and time). We need to introduce numerical simulations of combustion products flowing into free space of rocket motor. These effects are significant, and in certain moments real burning rate was even twice greater

then when it was determined from standardized burning law at higher burning pressures and temperature of 313 K.

4. CONCLUSION

Presented comparative analysis of four short-action solid rocket motors and particularly two (64 mm M80 „Zolja“ and 90 mm M79 „Osa“) which were mass consumed, shows how their specific features can affect design complexity.

When designed, a short-action solid rocket motor must fulfil following specific requirements:

- High burning pressure;
- High burn rate;
- „Plateau“ burning characteristics in operating range of pressure;
- “Mesa” burning characteristics over operating range of pressure;
- Low temperature sensitivity of the solid propellant (Low π_K);
- Reliable ignition;
- Short time of ignition propellant;
- Short ignition rise time;
- High specific impulse;
- Rocket motor must be operative at temperature range of -40^0C to $+60^0$C

Design performances of the burst diaphragm affect interior ballistic performances of short-action rocket motors. A greater thickness of the burst diaphragm can cause combustion oscillations, unforeseen peak pressure and solid propellant grain cracks. Thinner burst diaphragm impedes a proper ignition process that is obvious at temperature of 233 K (longer ignition rise time), and its influence should be explored as well.

Further research should be focused on more comprehensive igniter gases flow simulation through the inner space of the combustion chamber in order to determine a moment when entire exposed propellant grain surface was ignited.

Presented method for determination of characteristic points within burning time, based on derivative *dp/dt* of measured curve *p=f(t)*, enables that interior ballistic phases and their start and termination moments be more accurately determined.

LITERATURE

[1] http://upload.wikimedia.org/wikipedia/commons/c/c5/AT4_rocket_launcher.jpg

[2] Anon: *APILAS, armour piercing infantry light arm system*, Manurhin et Matra Societe, 1989. http://www.bellum.nu/armoury/GAPILAS.html, http://www.wammt.org/collections/weapons/apilas.htm

[3] http://www.israeli-weapons.com/weapons/missile_systems/anti-armor/b-300/B-300.html

[4] DRAGON round and tracker, Theory of operation and detailed functional description, Volume 1, Round, Report No. LO313, Mc Donnell Douglas Astronautics Company, 1978.

[5] H. Kentgens, H. P. Mackowiak and R. Schofn: Short-Action Solid Rocket Motors with Double-Base Propellants, Propellants, Explosives, Pyrotechnics 21, 118—126, 1996.

[6] Anon: Solid Rocket Motor Performance Analysis and Prediction, NASA Report SP 8039, May 1971, N72-18785.

[7] R. S. Fry: Solid propellant subscale burning rate analysis methods for U.S. and selected NATO facilities, The Johns Hopkins University, Chemical propulsion information agency, Columbia, Maryland, Januar 2002

[8] R. S. Fry: Solid propellant test motor scaling, The Johns Hopkins University, Chemical propulsion information agency, Columbia, Maryland, Septembar 2001

[9] J. Terzic: Prediction of idealized internal ballistic properties of a rocket motor with DB solid propellant, Master thesis, University of Sarajevo, Faculty of Mechanical Engineering, 2002.

[10] B. Zecevic: Influence of the variable radial acceleration to internal ballistics of rocket motors with DB propellants, Dissertation, University of Sarajevo, Faculty of Mechanical Engineering, 1999.

[11] K. M. Razdan and K. K. Kuo: Erosive Burning of Solid Propellants, Fundamentals of Solid-Propellant Combustion, Edited by Kuo K.K. and Summerfield, Progress in Astronautics and Aeronautics, Vol. 90, AIAA, 1984.

[12] B. Zečević and J. Terzic: Estimating current burning rate in standard ballistic rocket motor, 2nd International Symposium, Revitalization and Modernization of Production RIM ’99, ISBN 9958-624-06-0, Bihać, October 1999.

[13] B. Zecevic, J. Terzic and S. Serdarevic-Kadic: Effects of kinematics and mass characteristics of gas flow to basic rate burning of double-base rocket propellants, 3rd International Symposium, Revitalization and Modernization of Production RIM 2001, ISBN 9958-624-10-9, Bihać, September 2001.

[14] Michael A. Willcox, M. Quinn Brewster, K. C. Tang, D. Scott Stewart, and Igor Kuznetsov: Solid Rocket Motor Internal Ballistics Simulation Using Three-Dimensional Grain Burnback, Journal of Propulsion and Power Vol. 23, No. 3, May–June 2007

[15] J. Terzic and B. Zecevic: Prediction of performances of rocket motors. Program SPPMEF, University of Sarajevo, Defence Technologies Department, 2002.

[16] COMET Version 2.00 — Tutorials, ICCM — Institute of Computational Continuum Mechanics GmbH, Hamburg, March 2001.

[17] http://en.wikipedia.org/wiki/M72_LAW

[18] http://www.armyrecognition.com/forum/viewtopic.php?t=551

[19] http://www.mycity-military.com/Kopnena-vojska/Rucni-Protivoklopni-Raketni-Bacaci-tipa-RPG_4.html

[20] D. E. Coats,, J. N. Levine, N. S. Cohen, G. R. Nickerson, T. J. Tyson: A Computer Program for the Prediction of Solid Propellant Rocket Motor Performance, Volume 1, Air Force Rocket Propulsion Laboratory, July 1975